

Supporting Information for

Bifunctional additive 2-amino-3-hydroxypyridine for stable and high-efficiency tin-lead perovskite solar cells

Wentao Chen,^{1,2,3} Kuo Su,^{1,2} Yuqiong Huang,¹ Keith Gregory Brooks⁴, Sachin Kinge,⁵ Bao Zhang,^{1,3} Yaqing Feng,^{1,2,3} Mohammad Khaja Nazeeruddin,^{4*} Yi Zhang.^{4*}*

¹ School of Chemical Engineering and Technology, Tianjin University, Tianjin 300350, China.

² Tianjin Co-Innovation Center of Chemical Science and Engineering, Tianjin University, Tianjin 300072, China.

³ Haihe Laboratory of Sustainable Chemical Transformations, Tianjin 300192 (China)

⁴ Group for Molecular Engineering of Functional Material, Institute of Chemical Sciences and Engineering, École Polytechnique Fédérale de Lausanne, CH-1951 Sion, Switzerland.

⁵ Toyota Motor Corporation, Toyota Motor Technical Centre, Advanced Technology Div.; Hoge Wei 33, B-1930 Zaventem, Belgium.

Characterization and Measurements

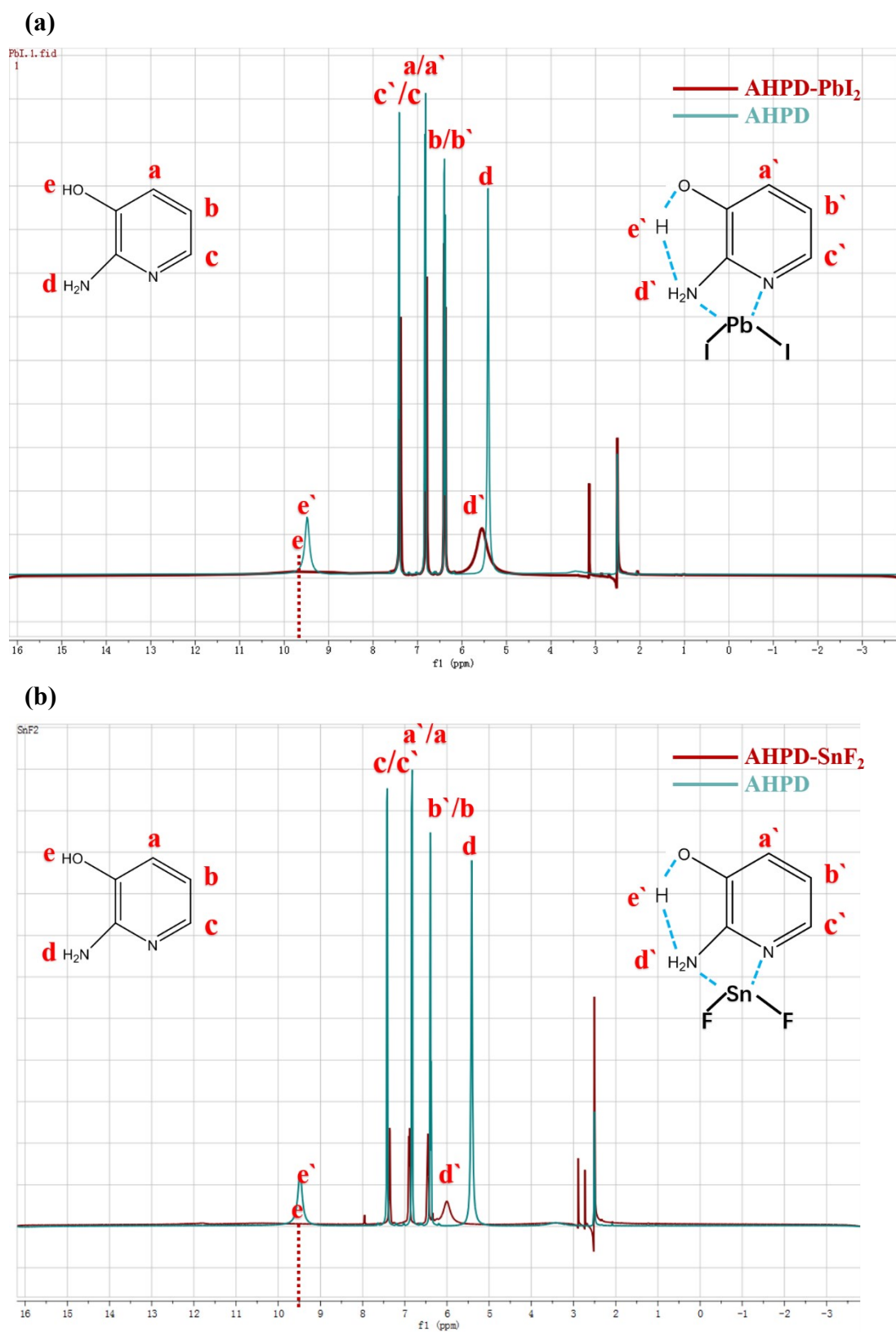
X-ray diffraction (XRD) patterns were obtained from a X'Pert Pro with Cu K α radiation. Fourier transform infrared (FTIR) spectra analysis was performed using an FTIR spectrometer (Nicolet6700, Thermo Electron Corporation, USA). A spectrophotometer (UV-1800, Shimadzu, JP) was used to measure the ultraviolet–visible (UV–vis) absorption spectra. A fluorescence spectrophotometer (FLS980, Edinburgh Instruments, U.K.) was used to measure the photoluminescence (PL). The steady-state PL (SSPL) was excited under 464nm with a monochromatized Xe lamp. The PL experiment's samples were fabricated on glass substrates. The surface and cross-sectional morphology of perovskite films were characterized by a field-emission scanning electron microscope (SEM, Regulus 8100, Hitachi, JP). Topography images and surface roughness deposited perovskite films were observed by an atomic force microscope (AFM, Dimension icon, Bruker, GER). Atomic force microscopy (AFM) and Kelvin probe force microscopy (KPFM) were tested in air without refreshed. The X-ray photoelectron spectroscopy (XPS) was carried out on an XPS analyzer (ESCALAB-250Xi, Thermo Fisher Scientific, USA) using 300 W Al K α radiation under a vacuum of 5×10^{-8} Pa.

The simulated solar illumination (AM 1.5 G, 100 mW cm $^{-2}$) was provided by a solar simulator (SS150, Zolix, CN) and calibrated with a calibrated Si reference cell. The current-density–voltage (J–V) curves of the PSCs were measured using a Keithley 2401 source meter with an active area of 0.0625 cm 2 defined by a non-reflective metal shadow mask at a scan speed of 100 mV s $^{-1}$ in an air atmosphere with 30-40% humidity. The stability of Sn–Pb PSCs was measured in an air atmosphere with 30-40% humidity and 20 \pm 5 $^{\circ}$ C with no encapsulation. The electrochemical impedance spectroscopy (EIS) was measured with an electrochemical workstation (CHI660D, CN) under dark conditions. External quantum efficiency (EQE) was obtained on a computer-controlled quantum efficiency instrument (QE-R, Enlitech).

In the SCLC measurement, the voltage of the trap-filled limit (VTFL) is defined as the voltage value at the intersection point of the two fitting lines representing the Ohmic contact and defect-filled regime. Furthermore, the defect density (N_{defect}) is calculated based on

$N_{defect} = \frac{2V_{TEL}\epsilon_r\epsilon_0}{qL^2}$, where the ϵ_r and ϵ_0 are the relative permittivities of the perovskite and the

vacuum, L is the thickness of the film, and q is the electron charge.



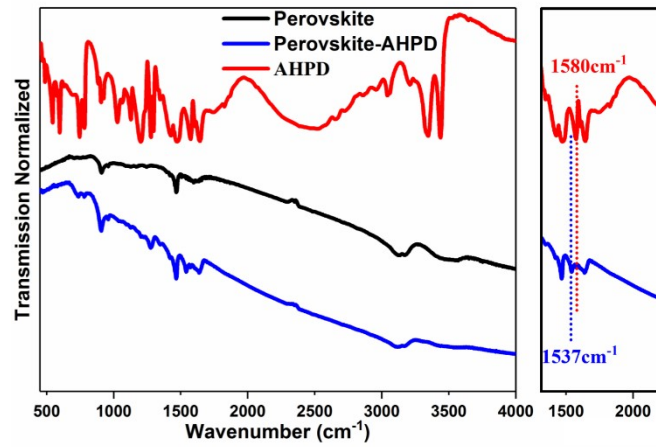


Figure S2. FTIR spectra of pristine AHPD, perovskite and perovskite coordinated with AHPD.

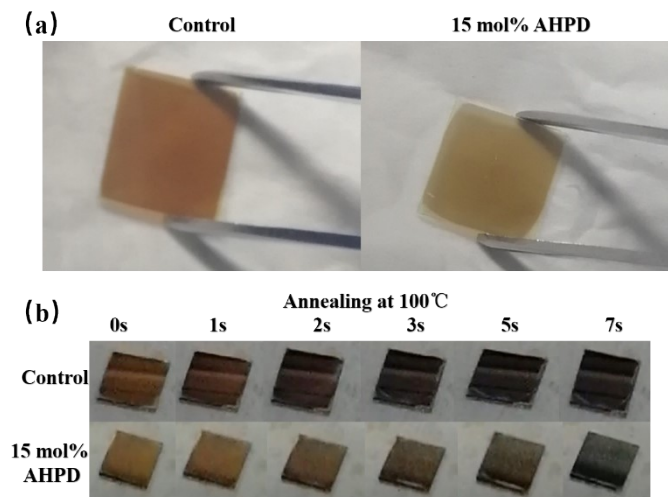


Figure S3. The perovskite films without and with AHPD before annealing(a). Photographs of $\text{FA}_{0.7}\text{MA}_{0.3}\text{Pb}_{0.5}\text{Sn}_{0.5}\text{I}_3$ films with and without AHPD during annealing at 100°C (b).

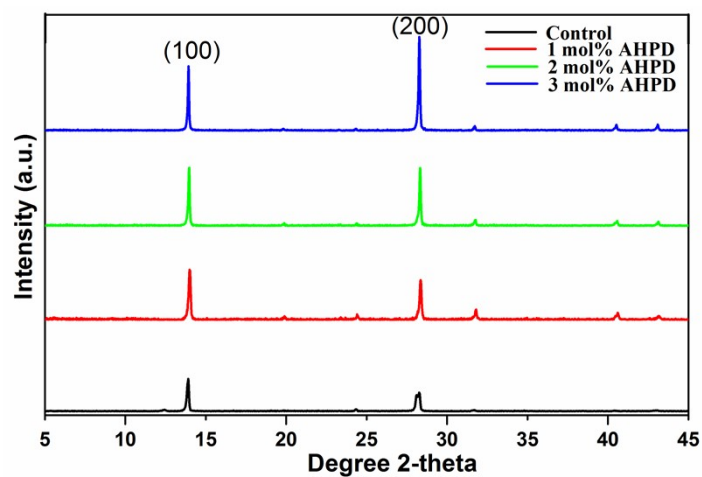


Figure S4. XRD pattern of the perovskite films with 0 mol%, 1 mol%, 2 mol%, 3 mol% AHPD, respectively.

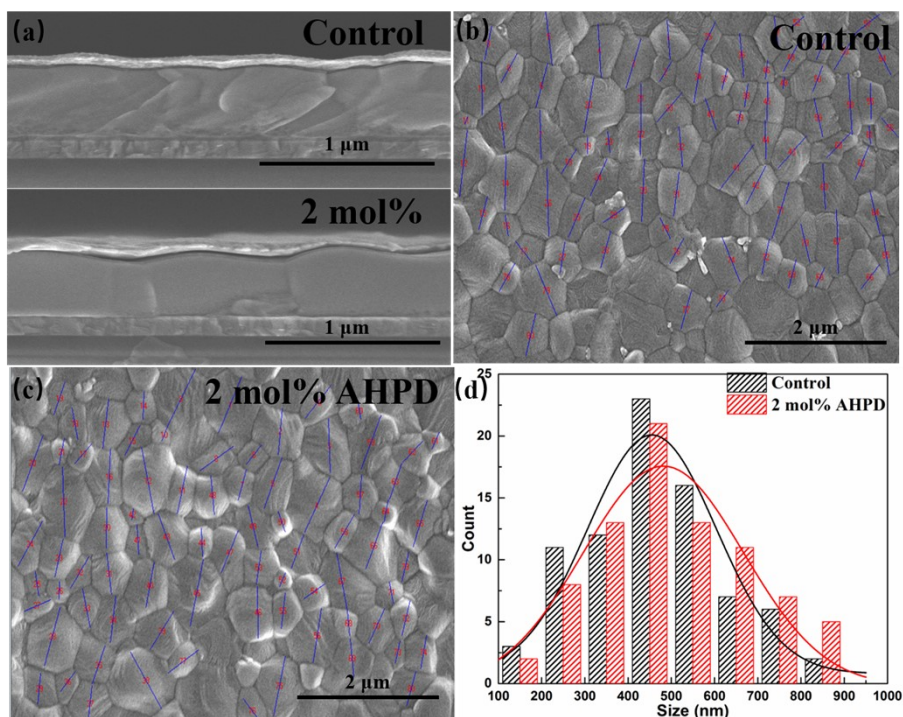


Figure S5. Cross-view SEM images(a) and grain size analysis of the control films(b) and the films with AHPD(c). And the corresponding statistical histograms(d).

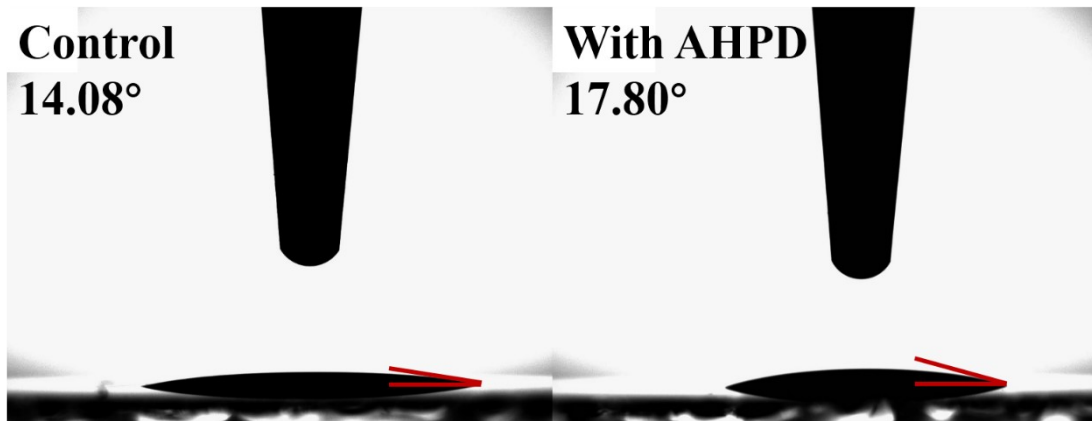


Figure S6. The contact angles between the perovskite precursor solutions (for the control and with AHPD, respectively) and the substrates.

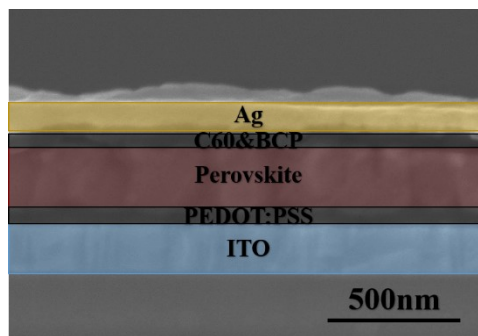


Figure S7. Schematic diagram and the representative cross-sectional SEM image of PSCs.

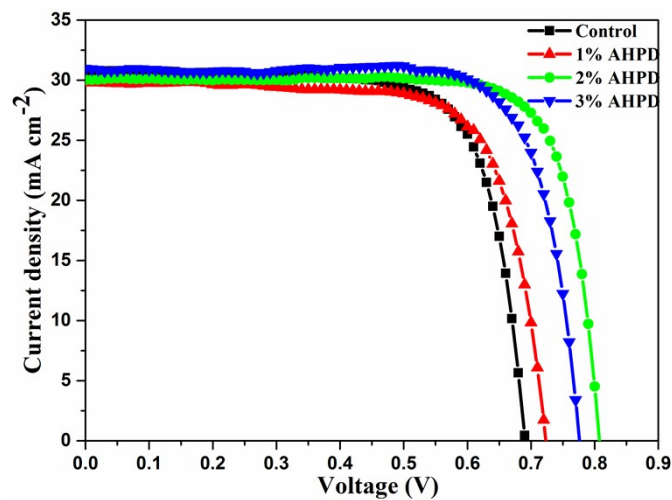


Figure S8. J–V curves of the champion devices with various AHPD concentrations under a reverse scan.

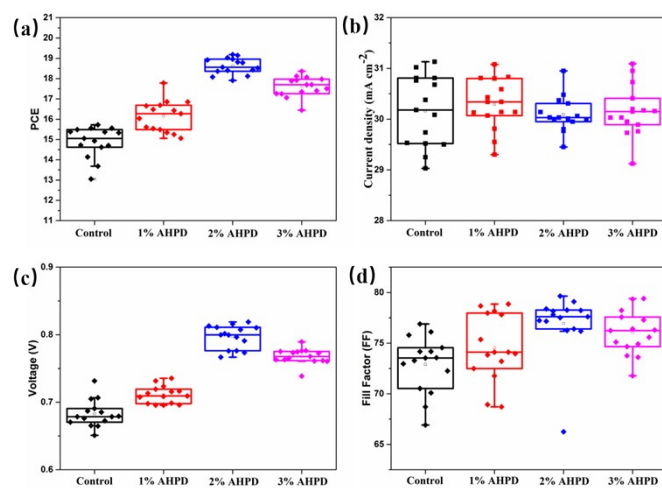


Figure S9. Photovoltaic performance of $\text{FA}_{0.7}\text{MA}_{0.3}\text{Pb}_{0.5}\text{Sn}_{0.5}\text{I}_3$ devices with various AHPD concentrations. The box lines indicate the standard deviation from 15 subcells, and the center represents the mean value.

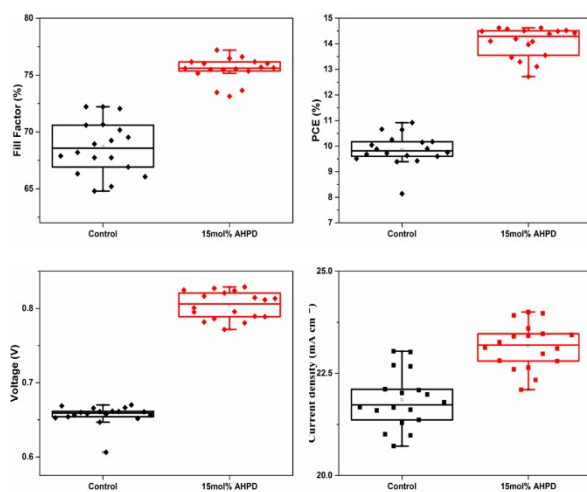


Figure S10. J_{SC} , V_{OC} , FF and PCE distribution of the control and AHPD-incorporated $\text{MAPb}_{0.6}\text{Sn}_{0.4}\text{I}_3$ device.

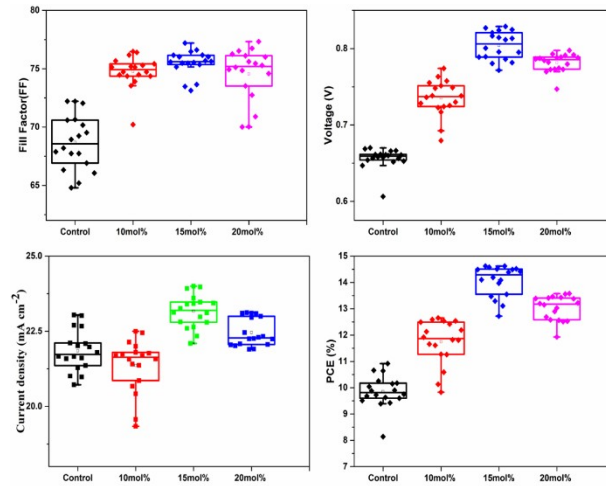


Figure S11. Photovoltaic performance of $\text{MAPb}_{0.6}\text{Sn}_{0.4}\text{I}_3$ devices with various AHPD concentrations. The box lines indicate the standard deviation from 45 subcells, and the center represents the mean value.

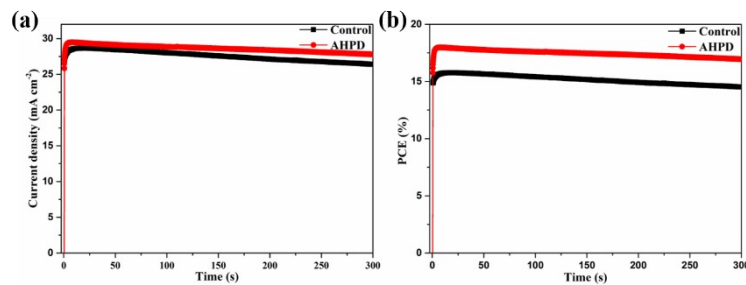


Figure S12. The stable output of photocurrent densities (a) and the steady-state PCEs (b) were measured at the maximum power point for the control and 2 mol% AHPD-incorporated $\text{FA}_{0.7}\text{MA}_{0.3}\text{Pb}_{0.5}\text{Sn}_{0.5}\text{I}_3$ devices, respectively.

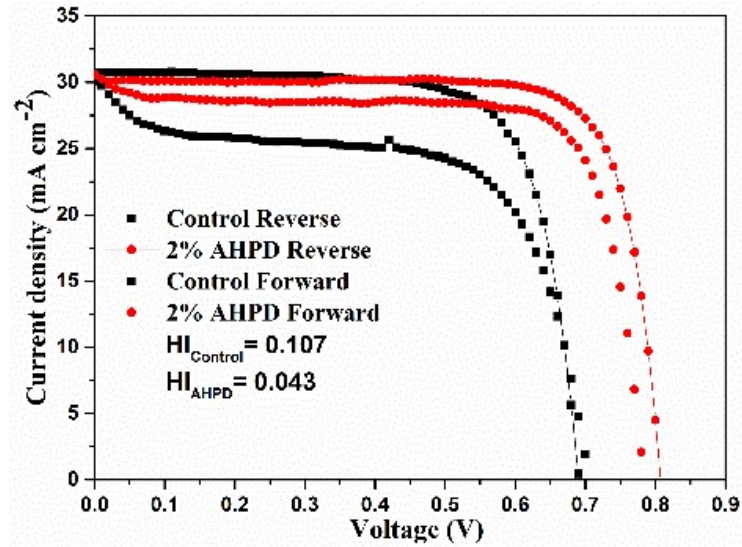


Figure S13. Hysteresis analysis of the AHPD-treated and control devices.

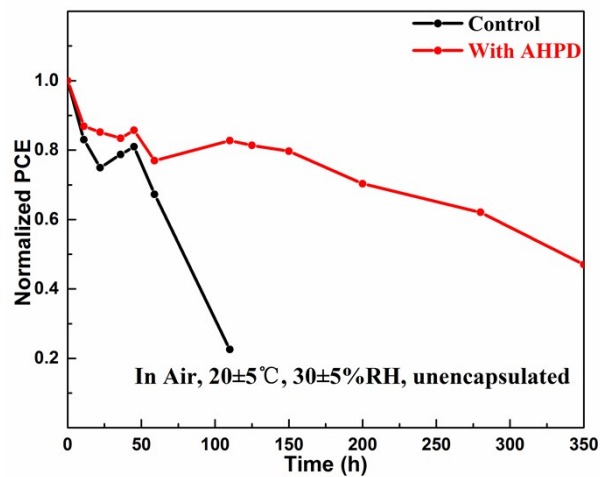


Figure S14. Evolution of PCE for the unencapsulated control and AHPD-incorporated devices with aging time after storage in the ambient atmosphere (30± 5% RH and 20 ± 5% °C).

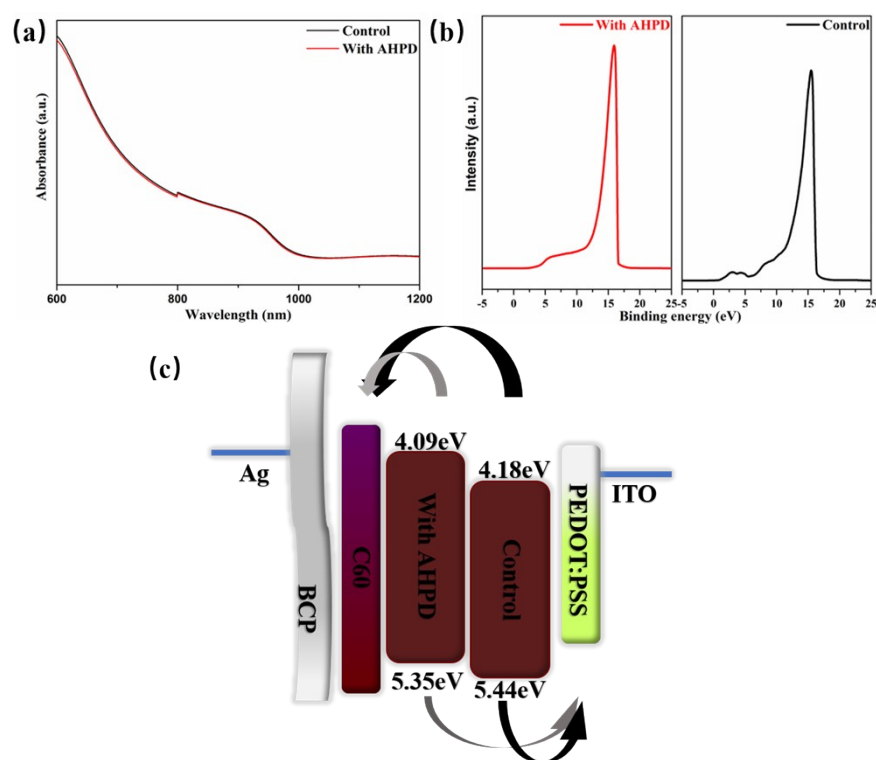


Figure S15. UV-vis absorbance spectra of the control and the film with 2 mol% AHPD(a). UPS spectra for control and AHPD-based devices(b). Energy-level diagram of perovskite solar cells, and HOMO and LUMO energy levels of AHPD-incorporated perovskite(c).

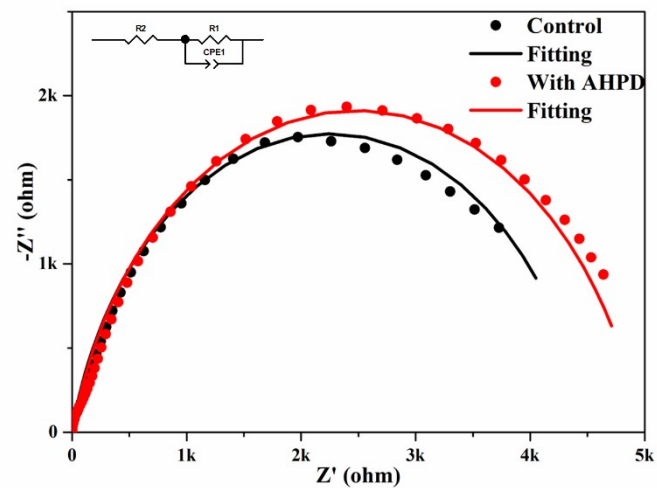


Figure S16. Nyquist plots curves of the control and the device with AHPD (with inset showing the equivalent circuit model for fitting the plots).

Table S1. Summary of Parameters for High-efficient $\text{MAPb}_x\text{Sn}_{1-x}\text{I}_3$ ($0.4 < x < 0.7$) Perovskite

Solar Cells Reported so far.

Perovskite film	J_{SC} (mA/cm²)	V_{OC} (V)	FF (%)	PCE (%)	Ref.
$\text{MAPb}_{0.4}\text{Sn}_{0.6}\text{I}_3$	20.5	0.77	63.10	10.00	[1]
$\text{MAPb}_{0.4}\text{Sn}_{0.6}\text{I}_3$	22.41	0.66	62.00	9.20	[2]
$\text{MAPb}_{0.5}\text{Sn}_{0.5}\text{I}_3$	20.64	0.58	60.00	7.27	[3]
$\text{MAPb}_{0.5}\text{Sn}_{0.5}\text{I}_3$	24.90	0.75	65.90	12.30	[4]
$\text{MAPb}_{0.5}\text{Sn}_{0.5}\text{I}_3$	25.50	0.84	67.00	14.40	[5]
$\text{MAPb}_{0.5}\text{Sn}_{0.5}\text{I}_3$	22.76	0.69	65.00	10.24	[6]
$\text{MAPb}_{0.5}\text{Sn}_{0.5}\text{I}_3$	26.10	0.73	69.00	15.61	[7]
$\text{MAPb}_{0.7}\text{Sn}_{0.3}\text{I}_3$	27.30	0.48	60.00	7.91	[8]
$\text{MAPb}_{0.7}\text{Sn}_{0.3}\text{I}_3$	20.30	0.77	66.40	10.41	[1]
$\text{MAPb}_{0.6}\text{Sn}_{0.4}\text{I}_3$	25.51	0.82	75.80	15.85	[9]
$\text{MAPb}_{0.6}\text{Sn}_{0.4}\text{I}_3$	17.80	0.75	61.60	8.20	[10]
$\text{MAPb}_{0.6}\text{Sn}_{0.4}\text{I}_3$	23.92	0.81	75.16	14.62	This work

Table S2. Photovoltaic parameters of devices with various AHPD concentrations as shown in Figure S9. (average values (avg) of 15 subcells)

		J_{sc} (max/avg)	V_{oc} (max/avg)	FF (max/avg)	PCE (max/avg)
MAPb _{0.6} Sn _{0.4} I ₃	Control	23.04/21.85	0.6566/0.6564	72.22/68.69	10.92/9.86
	10 mol%	22.50/21.37	0.7482/0.7351	75.13/74.76	12.65/11.75
	15 mol%	23.92/23.17	0.8133/0.8039	75.16/75.49	14.62/14.06
	20 mol%	23.10/22.46	0.7846/0.7816	74.93/74.56	13.58/13.08
FA _{0.7} MA _{0.3} Pb _{0.5} Sn _{0.5} I ₃	Control	30.68/30.08	0.6907/0.6761	74.18/74.16	15.72/15.05
	1 mol%	29.81/30.43	0.7234/0.7157	73.21/73.84	17.78/16.43
	2 mol%	30.03/30.06	0.8075/0.7996	79.10/78.16	19.18/18.78
	3 mol%	30.95/30.15	0.7761/0.7678	76.40/77.29	18.36/17.89

Reference

- [1] B. Zhao, M. Abdi-Jalebi, M. Tabachnyk, H. Glass, V. S. Kamboj, W. Nie, A. J. Pearson, Y. Puttisong, K. C. Gödel, H. E. Beere, D. A. Ritchie, A. D. Mohite, S. E. Dutton, R. H. Friend and A. Sadhanala, *Adv. Mater.*, **2017**, 29, 1604744.
- [2] S. Lee, D. W. Kang, *ACS Appl. Mater. Interfaces* **2017**, 9, 22432.
- [3] F. Hao, C. C. Stoumpos, R. P. H. Chang, M. G. Kanatzidis, *J. Am. Chem. Soc.* **2014**, 136, 8094
- [4] Li, Y., Sun, W., Yan, W., Ye, S., Rao, H., Peng, H., Zhao, Z., Bian, Z., Liu, Z., Zhou, H., & Huang, C. *Advanced Energy Materials*, 6(24).
- [5] Rajagopal, A., Yang, Z., Jo, S. B., Braly, I. L., Liang, P. W., Hillhouse, H. W., & Jen, A. K. Y. *Advanced Materials*, 29(34).
- [6] G. Lin, Y. Lin, H. Huang, R. Cui, X. Guo, B. Liu, J. Dong, X. Guo and B. Sun, *Nano Energy*, **2016**, 27, 638–646.
- [7] A. Rajagopal, P.-W. Liang, C.-C. Chueh, Z. Yang and A. K.-Y. Jen, *ACS Energy Lett*, **2017**, 2, 2531–2539.
- [8] K. Hamada, R. Tanaka, M. A. Kamarudin, Q. Shen, S. Iikubo, T. Minemoto, K. Yoshino, T. Toyoda, T. Ma, D.-W. Kang and S. Hayase, *ACS Appl. Mater. Interfaces*, **2020**, 12, 17776–17782.
- [9] Zhu, Z., Li, N., Zhao, D., Wang, L., & Jen, A. K. Y. *Advanced Energy Materials*, 9(7).
- [10] M. M. Tavakoli, S. M. Zakeeruddin, M. Grätzel, Z. Y. Fan, *Adv. Mater.*, **2018**, 30, 1705998.